ADVANCED FUNCTIONAL MATERIALS
www.afm-journal.de

Modulated Thermoelectric Properties of Organic Semiconductors Using Field-Effect Transistors

Fengjiao Zhang, Yaping Zang, Dazhen Huang, Chong-an Di, Xike Gao, Henning Sirringhaus, and Daoben Zhu**

Organic thermoelectric materials, which can transform heat flow into electricity, have great potential for flexible, ultra-low-cost and large-area thermoelectric applications. Despite rapid developments of organic thermoelectric materials, exploration and investigation of promising organic thermoelectric semiconductors still remain as a challenge. Here, the thermoelectric properties of several p- and n-type organic semiconductors are investigated and studied, in particular, how the electric field modulations of the Seebeck coefficient in organic field-effect transistors (OFETs) compare with the Seebeck coefficient in chemically doped films. The extracted relationship between the Seebeck coefficient (S) and electrical conductivity (σ) from the field-effect transistor (FET) geometry is in good agreement with that of chemically doped films, enabling the investigation of the trade-off relationship among σ, S, carrier concentration, and charging level. The results make OFETs an effective candidate for the thermoelectric studies of organic semiconductors.

1. Introduction

Thermoelectric materials are of great interest for applications in power generation from waste heat using the Seebeck effect, in addition to being useful for refrigeration by means of the Peltier effect.[1–6] Benefiting from materials sciences and engineering optimization of thermoelectric devices, the main figure of merit, $ZT = S^2\sigma T/\kappa$, has improved dramatically in the past few years, where S is the Seebeck coefficient, σ is the electrical conductivity, T is the absolute temperature, and κ is the thermal conductivity. Organic semiconductors are now considered as attractive thermoelectric candidates owing to their intrinsically low thermal conductivity and potential low cost associated with their ease of low-temperature processing.[7–14] However, organic semiconductors typically suffer from low carrier concentration and electrical conductivity, both of which impede their direct applications in thermoelectric generators. Chemical and electrochemical doping are two key strategies for maximizing the thermoelectric properties of organic semiconductors by modulating the free-carrier concentration and changing the carrier mobility.[10,11,13–18] By implementing chemical doping of poly(3,4-ethylenedioxy-thiophene) (PEDOT) with poly(styrenesulfonate) and electrochemically fine-tuning of oxidation level,[13,14] impressive thermoelectric performances were achieved, demonstrating great potential of organic materials in thermoelectric applications.

Exploration of promising thermoelectric materials is a fundamental issue in organic thermoelectronics. So far, only a limited number of organic thermoelectric materials have been reported.[7–9,19–24] Unfortunately, chemical and electrochemical doping cannot always be used as an efficient way to explore organic thermoelectric materials because of limited applicability to achieve consistently a high electrical conductivity in a wide range of different organic semiconductors.[17] Moreover, the chemical doping of organic semiconductors might lead to a reduced hopping rate as a result of a possible increase in the structural disorder and a broadening of the density of states (DOS), thereby decreasing the carrier transport in organic semiconductors.[10,13,25]

In a typical organic transistor, however, the gate voltage induces the charged states at the dielectric–organic layer interface, leading to a *quasi*-2D conductive channel with limited influence on the intermolecular distance. Once a temperature differential ΔT is applied across source-drain electrodes, carries within the conductive channel diffuse from the hot electrode to the cold one and an electric field (V_{therm}) build up. The Seebeck coefficient (S), which is influenced by the carrier concentration, can be extracted by the relation $S = V_{\text{therm}}/\Delta T$. Since the carrier concentration can be precisely controlled by the pulsed voltage, many key parameters including the electrical conductivity, molecular charging level, and even Seebeck

F. Zhang, Y. Zang, D. Huang
University of Chinese Academy of Sciences
Beijing 100049, P.R. China
F. Zhang, Y. Zang, D. Huang, Dr. C. A. Di, Prof. D. B. Zhu
Beijing National Laboratory for Molecular Sciences
Key Laboratory of Organic Solids
Institute of Chemistry
Chinese Academy of Sciences
Beijing 100190, P.R. China
E-mail: dicha@iccas.ac.cn; zhudb@iccas.ac.cn
Prof. X. K. Gao
Laboratory of Synthetic and Self-Assembly Chemistry for Organic Functional Molecules
Shanghai Institute of Organic Chemistry
Chinese Academy of Sciences CAS
Shanghai 200032, P.R. China
Prof. H. Sirringhaus
Cavendish Laboratory
University of Cambridge
JJ Thomson Avenue, Cambridge CB3 0HE, UK

DOI: 10.1002/adfm.201404397

coefficient can be modulated in a single transistor. This allows the investigation of the Seebeck coefficient as a function of carrier concentration (N_{ind}) and electrical conductivity by simply varying the gate voltage.[26–28] Such kind of S–σ and S–N_{ind} trade-off relationship study of different organic semiconductors can thus facilitate insight understanding of molecular engineering of organic thermoelectric materials and achievement of maximum thermoelectric properties. In addition, the specific contribution of field-induced charge species to the thermoelectric properties can be studied using transistor geometry.[27–32]

Although in principle organic transistors can serve as a platform for the thermoelectric studies of organic semiconductors, investigation on field-modulated thermoelectric properties of organic semiconductors is still an attractive topic because: i) a comparison between the thermoelectric properties of chemically doped semiconductors and the performances extracted from organic field-effect transistors (OFETs) is required to provide an direct evidence that investigation of field-effect- modulated thermoelectric performance of organic semiconductors can plays an important role in the study of organic thermoelectric materials; ii) the low carrier concentration and electrical conductivity in typical OFETs make investigation of S–σ trade-off relationship in a short conductivity range and limit its application in probing thermoelectric properties of organic semiconductors. These challenges make systematic investigation on field-effect-modulated thermoelectric properties of organic semiconductors highly desired.

Here, we experimentally find that the field-induced charged species in both p- and n-type OFETs can dominate the thermoelectric properties of organic semiconductors. Several semiconductors in field-effect transistor (FET) geometry with SiO_2 and electrolyte dielectric layer exhibit impressive power factor over a wide range of conductivities from 10^{-4} S cm^{-1} to 100 S cm^{-1}. These thermoelectric performances are consisted with that of chemically doped films, allowing effective investigation of the S–σ trade-off relationship of organic semiconductors. These features, together with the need to efficiently screen potentially hundreds of high mobility organic semiconductors, make OFET promising candidate for investigating the thermoelectric properties of organic semiconductors.

2. Results and Discussion

2.1. Thermoelectric Characterization of OFETs

OFETs based on *p*-type poly(2,5-bis(3-alkylthiophen-2-yl) thieno[3,2-b]thiophene) (PBTTT), poly(3-hexylthiophene) (P3HT), and *n*-type naphthalene diimides derivatives, NDI3HU-DTYM2, and NDI(2OD)(4t-BuPh)-DTYM2 (**Figure 1**a,b) were fabricated. The typical OFET device structure for thermoelectric property measurement is shown in Figure 1a, while the device fabrication and measurements are described in experimental section. Different from typical OFETs with channel length of 5–100 µm, a large channel length ranging from 200 to 600 µm was utilized to ensure an appropriate temperature difference across source-drain electrodes. In addition to the typical electrical investigation, we studied their gate voltage-dependent thermoelectric characteristics, namely the electrical conductivity (σ), Seebeck coefficient (S), and power factor ($P = S^2\sigma$).

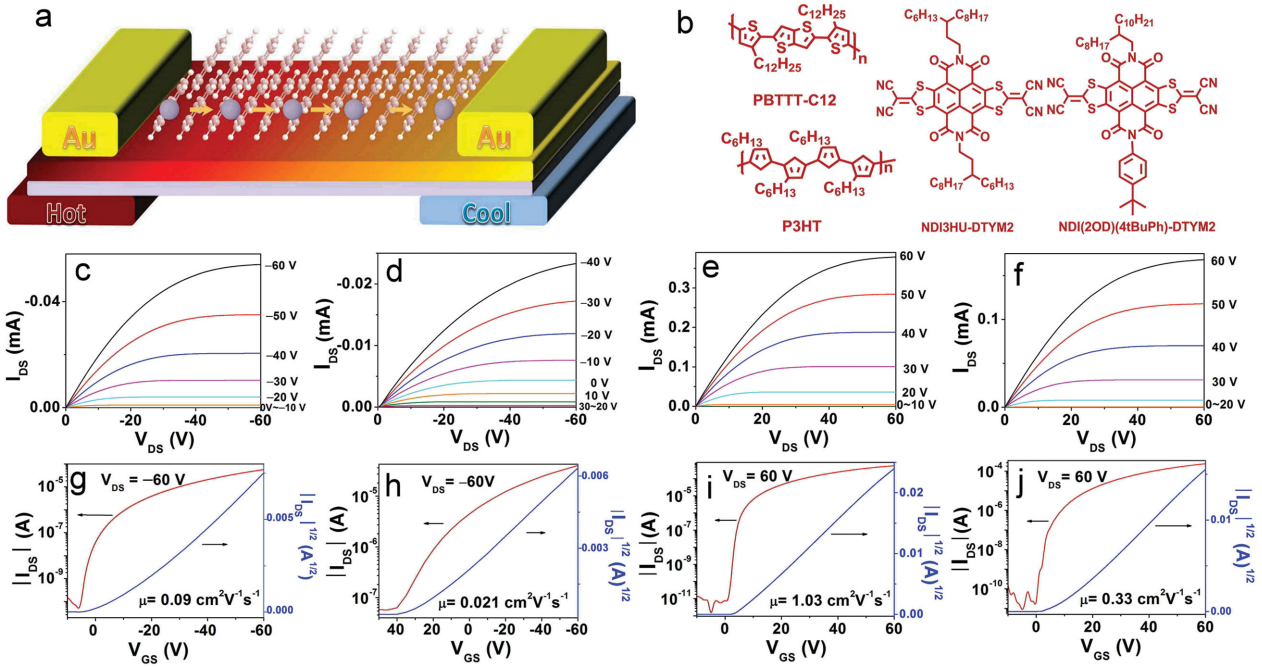

Figure 1. a) Illustrative schematic of OFET structure for thermoelectric measurement. b) Molecular structures of organic semiconductors. Output and transfer characteristics of OFETs based on c,g) PBTTT; d,h) P3HT; e,i) NDI3HU-DTYM2; and f,j) NDI(2OD)(4t-BuPh)-DTYM2. The channel length and width are 400 µm and 1.2 cm, respectively.

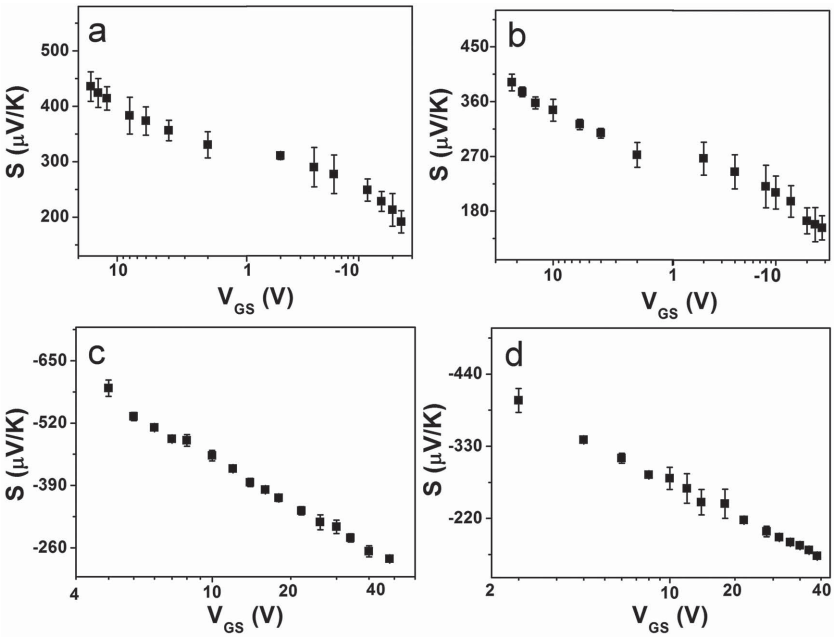

Figure 2. Seebeck coefficient in film OFETs based on a) PBTTT, b) P3HT, c) NDI3HU-DTYM2, and d) NDI(2OD)(4t-BuPh)-DTYM2, as a function of gate voltage.

The device characteristics of bottom gate OFETs were show in Figure 1c–j. The output curve and transfer curve indicated that the operation of fabricated OFETs is conformed to standard FET theory. All the devices exhibited well-defined output and transfer characteristics with field effect mobility ranging from 0.02 to 1.03 $cm^2\ V^{-1}\ s^{-1}$ in spite of the large channel length (200–600 μm). When applying a temperature gradient across the source-drain electrodes in the presence of an applied gate bias, it was straightforward to measure the Seebeck coefficient and its field dependence for different organic semiconductors. **Figure 2** shows the measured Seebeck coefficient in OFETs geometry on SiO_2 dielectric layer at room temperature. The Seebeck coefficient was found to decrease with increasing gate voltage over the measured range for all materials. The measured Seebeck coefficients of PBTTT and P3HT decreased from 450 and 390 to 150 μV K^{-1} and 100 μV K^{-1}, respectively, when the gate voltage changed from 20 to −28 V (Figure 2a,b). As for the *n*-channel materials, the Seebeck coefficient of NDI3HU-DTYM2 and NDI(2OD)(4t-BuPh)-DTYM2 changed from −600 and −400 to −240 μV K^{-1} and −160 μV K^{-1}, respectively, upon increasing gate voltage from 2 to 40 V (Figure 2c, d,). This result provides clear evidence that the Seebeck coefficient of these organic semiconductors can be well modulated by the gated electric field in OFETs.[28]

To make a direct comparison between the field-modulated and chemically doped thermoelectric properties of organic semiconductors, we also studied the thermoelectric properties of chemically doped PBTTT and P3HT (**Figure 3**). It should be noted that the thermoelectric properties of chemically doped organic semiconductors are greatly affected by the properties of the dopants as well as the doping methods.[11,13,33–37] Since we are not intend to focus on the systematic investigation of chemical doping, the chemical doping of PBTTT with $NOPF_6$ and surface proton doping of P3HT by graphene oxide were performed according to previous reports to make a preliminary comparison of the field-modulated and chemically doped thermoelectric properties of organic semiconductors.[25,33] Figure 3a,b summarize the *S*–σ of PBTTT and P3HT obtained by both electric field modulation and chemical doping, where for the OFET measurements, the electrical conductivity σ was calculated by assuming that the conductive channel has a thickness of two molecular layers (3.4–4.0 nm) (Figure S1, Supporting Information). Full film thickness and 3.4 nm were used to calculate the conductivity of chemically doped films of PBTTT and P3HT, respectively, owing to the interfacial doping nature of P3HT by graphene oxide.[25,33] Meanwhile, the Seebeck coefficient decreases proportionally to log σ when the conductivity changed from 10^{-4} to 0.1 S cm^{-1} for both cases. It was found that the *S*–σ trade-off relationship trend extracted from FET measurements was in good accordance with the trend obtained

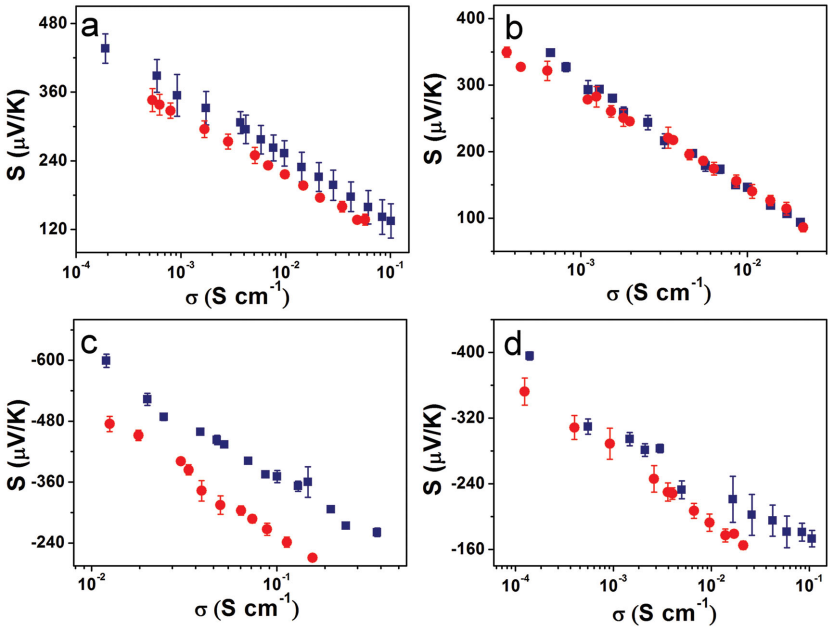

Figure 3. Thermoelectric properties versus different organic semiconductors. Seebeck coefficients (navy filled squares for materials in OFET geometry and red filled dots for chemical doped materials) as a function of conductivity for a) PBTTT, b) P3HT, c) NDI3HU-DTYM2, and d) NDI(2OD)(4t-BuPh)-DTYM2.

from chemically doped semiconductors. It should be noted that the chemical doping performance in the result is consistent with previous reports.[34,35] A slight change in Seebeck coefficient should be ascribed to the different counterions in chemical doping (Table S1, Supporting Information).

N-channel OFETs based on NDI3HU-DTYM2 and NDI(2OD)(4t-BuPh)-DTYM2 were investigated with the same method (Figure 3c, d). NDI3HU-DTYM2 exhibits a remarkable Seebeck coefficient varying from −600 to −240 μV/K when the electrical conductivity changes from 10^{-2} to 0.4 S cm^{-1}. The sign of the Seebeck coefficient is consistent with the electron transport nature of n-type materials. NDI(2OD)(4t-BuPh)-DTYM2 exhibits similar S–σ trend with a slightly lower Seebeck coefficient of −400 to −160 μV K^{-1}. We then doped NDI3HU-DTYM2 and NDI(2OD)(4t-BuPh)-DTYM2 with NH_3 and NH_2NH_2 to evaluate the differences between field-modulation and chemical doping (Figure S2 and S3, Supporting Information). Similar to p-channel polymers, the S–σ relationship of NDI3HU-DTYM2 and NDI(2OD)(4t-BuPh)-DTYM2-based OFETs was consistent with the result obtained from chemical doping. For a typical OFET, the charge carriers accumulate and transport at the conductive channel, which is located at the few molecular layers near the dielectric/organic layer interface. Given an ultrathin feature (10 nm) of gate voltage-modulated channel, the measurement of the in-plane thermal conductivity in OFETs is a great challenge. Here, the power factor, instead of ZT, is used to evaluate the thermoelectric properties of the organic semiconductors. Figure S4 (Supporting Information) summarized the thermoelectric power factor as a function of conductivity for four semiconductors. A power factor of 2.5 μW m^{-1} K^{-2} (Figure S4c, Supporting Information) is achieved at a conductivity of 0.4 S cm^{-1} for NDI3HU-DTYM2, which appears that NDI3HU-DTYM2 is a promising *n*-type thermoelectric material.

For semiconductors in FET geometry, the Seebeck coefficient varies with the applied gate field by the modulation of the carrier concentration in the quasi-2D conductive channel and, hence, the Fermi level position, E_F, of the molecules. We calculated the total induced charge-carrier density from $N_{ind} = C_{ox}(V_{GS}\text{-}V_T)/e$, where C_{ox} is capacitance of the dielectric layer, V_T is the threshold voltage, V_{GS} is the gate voltage.[28] The Seebeck coefficient of different organic semiconductors decreases proportionally to log(N_{ind}) for P3HT- and PBTTT-based OFETs with a similar trend (**Figure 4**a). However, NDI3HU-DTYM2 and NDI(2OD)(4t-BuPh)-DTYM2 suffer from a considerable difference in the S–N_{ind} relationship because of their differences in molecular packing and charge transport properties.

By using the known intermolecular stacking of the organic semiconductors and calculated charge-carrier density, the charging level, which is defined as the ratio of the number of carriers to the repeat units of polymers or molecular number of small molecules, could be estimated (Figure S5, Supporting Information).[36] Figure 4b shows the Seebeck coefficient as a function of charging level for different semiconductors. All the semiconductors possess a low charging level ranging from 0.02% to 5% even at high gate voltages. Similar to the S–N_{ind} relationship, the Seebeck coefficient decreases proportionally with the charging level for different semiconductors. Although these devices possess comparable carrier concentrations, a higher charging level (0.1%–5%) was obtained for n-channel devices relative to the p-channel ones (0.02%–0.7%), owing to the differences in the charged species and intermolecular stacking for different materials. The relatively lower charging level of P3HT and PBTTT compared to those of NDI3HU-DTYM2 and NDI(2OD)(4t-BuPh)-DTYM2 might be an important reason for their low power factors in FET geometry. Since the carrier concentration and charging level are very difficult to extract for the chemically doped organic semiconductors, the obtained relationship of the electrical conductivity, carrier concentration, charging level, and Seebeck coefficient constitutes a feature of thermoelectric studies with FET geometry.

2.2. Thermoelectric Properties of OFETs with Electrolyte Dielectric Layers

In spite of field modulation of the Seebeck coefficient and electrical conductivity, a disadvantage of the FET measurements of typical OFETs is that the carrier densities that can be achieved are not as high as the regime where most thermoelectric devices work, so one can only probe the low carrier density regime with low conductivity (<1 S cm^{-1}). In comparison, the electrolyte-gate OFETs can display high conductivity with low operating voltages because of ultra-high capacitance (1-100 μF cm^{-2}) of the electrolyte dielectric layer. Therefore, high carrier density and a metallic conductivity (≈1000 S cm^{-1}) in P3HT can even be obtained.[38] Here, by introducing an electrolyte dielectric layer of poly(methyl methacrylate (PMMA)/1-ethyl-3-methylimi dazolium bis(trifluoromethylsulfonyl)imide ([EMIM][TFSI]),[39] a high capacitance of 28 μF cm^{-2} at low frequency of 1 Hz was achieved (**Figure 5**). It thus enables realization of low operating voltage lower than 3 V. All the devices exhibited well-defined output and transfer characteristics with maximum field-effect mobility of up to 5.6 and 4.8 cm^2 V^{-1} s^{-1} for PBTTT- and P3HT-based OFETs, respectively. The outstanding performances of electrolyte-based devices allow effective investigation of thermoelectric properties of *p*-channel polymers in relatively high carrier density regime.

Different from typical OFETs with SiO_2 dielectric layer, the devices with electrolyte

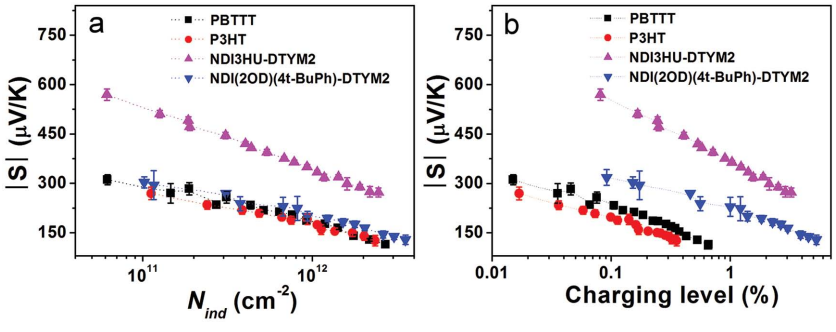

Figure 4. Seebeck coefficient as a function of a) carrier density N_{ind} and b) charging level for the semiconductor in OFETs geometry, respectively.

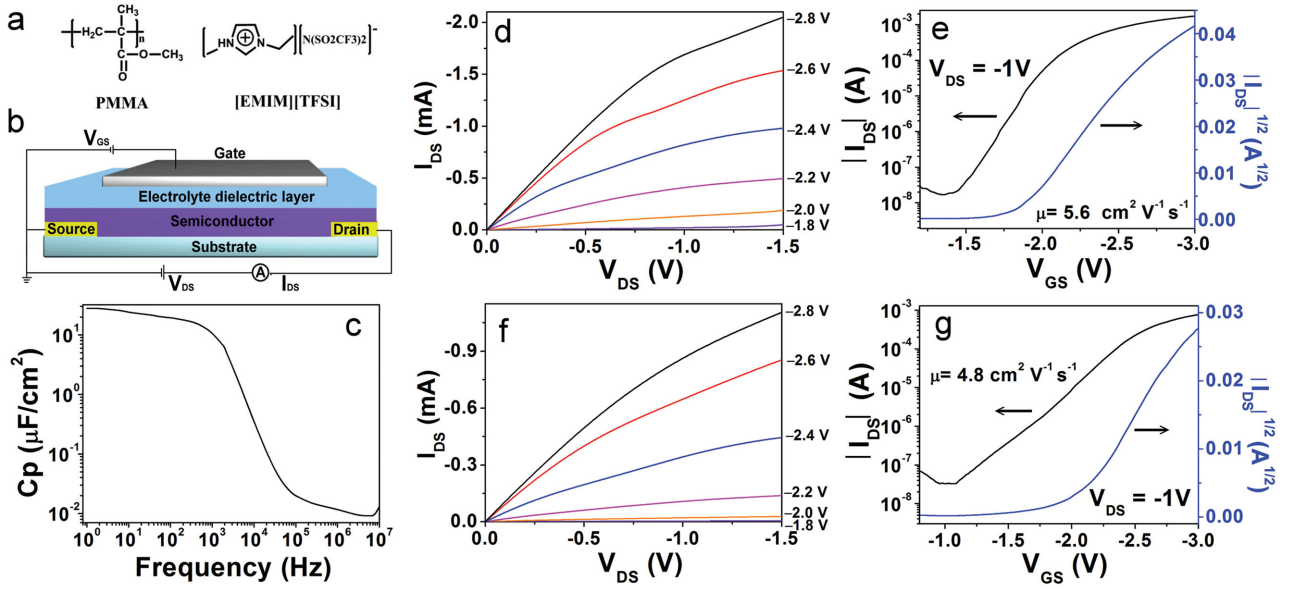

Figure 5. a) Molecular structure of PMMA and [EMIM][TFSI]. b) Schematic diagram of a top-gate electrolyte dielectric OFET. c) Frequency-dependent capacitance of PMMA/[EMIM][TFSI] electrolyte dielectric layer. d,f) Output and e,g) transfer characteristics of electrolyte OFETs based on d,e) PBTTT and f, g) P3HT.

dielectric layer can induce electrochemical doping of the active film.[16,35,40–44] **Figure 6** summarized the relationship of S–σ, P–σ, S–N_{ind}, and S-charging level of PBTTT- and P3HT-based OFETs with electrolyte dielectric layers. It should be noted that the electrical conductivity of PBTTT can be improved to 100 S cm^{-1} by using PMMA/[EMIM][TFSI] dielectric layer. The value is three orders of magnitude higher than the conductivity achieved by using SiO_2 dielectric layer. Moreover, benefiting from the high N_{ind} (2×10^{13} cm^{-2}) induced by the ultra-high capacitance of PMMA/[EMIM][TFSI] dielectric layer, we realized a high charging level of 5.2% (Figure 6c,d) for PBTTT. It is important to note that both the conductivity and carrier density are comparable with the values of chemically doped materials where most thermoelectric devices work.

Interestingly, the Seebeck coefficient of PBTTT in these electrolyte devices retains a high value of 150–50 μV K^{-1} even at a high conductivity of >1 S cm^{-1} (Figure 6a). It is comparable to the Seebeck coefficient in the low conductivity regions (<0.1 S cm^{-1}) in typical SiO_2 dielectric devices. Taking advantage of the high Seebeck coefficient and electric conductivity, a maximum power factor of 22 μW m^{-1} K^{-2} was achieved. This value is one order higher than the common observed values in typical OFETs and is superior to the power factor of chemically doped PBTTT (14 μW m^{-1} K^{-2}) under optimized condition.[35] Such kind of positive influence on the thermoelectric properties could be further verified by P3HT devices with electrolyte dielectric layer. For the P3HT devices with PMMA/[EMIM][TFSI] layer, high N_{ind} and charging level of up to 6×10^{13} cm^{-2} and 9.6% are successfully achieved (Figure 6c,d). It thus facilitates the enhancement of the conductivity and power factor. As a result, the device exhibits a maximum conductivity of 38 S cm^{-1} and optimized power factor of 40 μW m^{-1} K^{-2}, which is higher than that of chemically doped P3HT (30 μW m^{-1} K^{-2}).[35]

2.3. Discussion

In general, the key thermoelectric parameters, including the Seebeck coefficient and conductivity, are measured with chemically doped bulk materials across macroscopic distances. In a typical OFET, however, the channel length ranges from a few micrometers to hundreds of micrometers, and carrier transport usually occurs in the conductive channel that located on the few molecular layers near the dielectric layer. Such electric-field-induced interfacial doping in OFETs can be verified by the independence of thermoelectric properties on the film thickness (Figure S6, Supporting Information). It is therefore very important to compare the thermoelectric performance obtained by different doping approaches. Interestingly, for all semiconductors including PBTTT, P3HT, NDT3HU-DTYM2, and NDI(2OD)(4t-BuPh)-DTYM2, the S–σ trade-off relationship trends extracted from FET measurements were in good accordance with the trends obtained from chemically doped samples. However, we obtained slightly higher Seebeck coefficient at a fixed electrical conductivity, which were extracted from FET measurements, than those of chemically doped ones for PBTTT, NDT3HU-DTYM2, and NDI(2OD)(4t-BuPh)-DTYM2 (Figure 3a,c,d). It is worth noting that P3HT exhibited very similar Seebeck coefficient at fixed electrical conductivity in different measurements (Figure 3b).

For PBTTT, P3HT, and NDI-DTYM2 derivatives, the electric conductivity increases with increasing temperature range from 200 to 330 K,[10,25,45] which suggest phonon-assisted hopping mechanism of these semiconductors.[12,46,47] In the hopping transport, the Seebeck coefficient is proportional to E–E_F[16,48] and can be written as

$$S = \frac{k_B}{e} \int \frac{E_F - E}{k_B T} \frac{\sigma(E)}{\sigma} dE \quad (1)$$

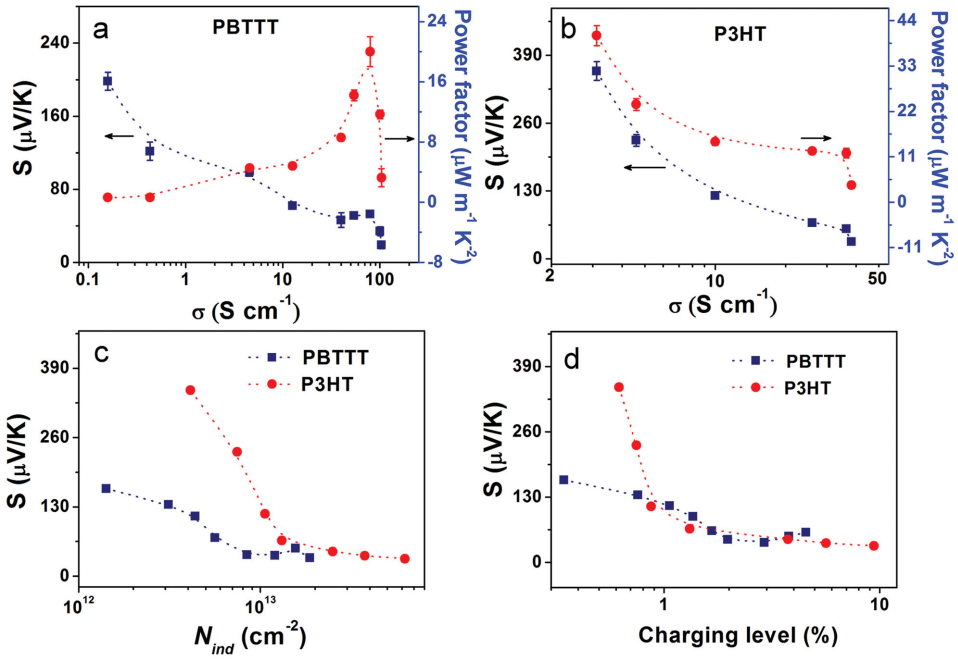

Figure 6. Thermoelectric properties of OFETs with electrolyte dielectric layers. Seebeck coefficients (navy filled squares) and thermoelectric power factor (red filled dots) as a function of conductivity for a) PBTTT and b) P3HT. c) and d) show the Seebeck coefficient as a function of carrier density N_{ind} and charging level for the semiconductor in OFETs geometry, respectively.

where k_B is the Boltzmann constant, e is the electron charge, E_F is the Fermi energy of the materials, $\sigma(E)$ is the electric conductivity, σ is the conductivity, T is the absolute temperature, E is the energy level occupied by the carrier.[9,16,27,28,48] Using the general expression of E_F and electron density, the above equation can be simplified to

$$S = C(\ln N_C - \ln n + A) \quad (2)$$

where n is the carrier concentration, N_C is the effective DOS and is the so-called heat-of-transport constant, C and A represent the fitting parameter and a scattering factor of the semiconductor, respectively.[27,48,49] From the above equation, Seebeck coefficient decreases with increasing carrier concentrations, which agrees well with the results observed in our studies. In a FET, the carrier concentration can be modulated by applying a varied gate voltage. Since increased charge carrier accumulate and transport in the conductive channel with enhanced gate voltage, the S decreases logarithmically with increasing gate voltage. The near-liner relationships between S and log σ are consistent with previous reports and may be explained by the Holstein–Hubbard molecular model (MCM).[34,50]

Because DOS is related to the density of the molecules in thin film of an organic semiconductor,[27,48,51] the Seebeck coefficient is affected by intermolecular packing. Close intermolecular packing is favorable to facilitate improvement in both N_C and the charge transport property. In chemical doping, the dopant inions usually diffuse into the film.[46] Therefore, the introduction of a chemical dopant might leads to a change in the intermolecular packing. In case of PBTTT and P3HT, doping with $NOPF_6$ and TFSI anions results in an increase in the lamellar distance by 0.2 nm.[10,25] Although an accurate N_C value of chemically doped PBTTT cannot be calculated at moment, a lower N_C value can be expected. This in turn lowers the Seebeck coefficient and carrier mobility at a fixed carrier concentration. In contrast, the electric-field-induced doping in FETs can modulate the doping level and energy level of organic semiconductors with limited change in the intermolecular packing and hence maintained N_C.[36] We thus attribute the superior thermoelectric properties of PBTTT, NDT3HU-DTYM2, and NDI(2OD)(4t-BuPh)-DTYM2 obtained in the FET geometry to the avoidance of an obvious increase in the intermolecular tunneling distance. As for P3HT, interfacial doping of the active film is performed by using graphene oxide in this experiment, which contributes to a comparable Seebeck coefficient with gate modulated. Therefore, it can be concluded that the slight difference in Seebeck coefficient between FET measurements and chemically doped films can be ascribed to varied doping mechanisms of chemical and electric-field-induced doping. Field-effect doping of organic semiconductors via OFETs can serve as an effective way for thermoelectric studies of different materials.

Different from typical OFETs with SiO_2 dielectric layer, there is the potential for bulk doping using electrolyte dielectric layer. In fact, several groups show that using electrolyte dielectric layer can either lead to bulk and/or interfacial transport.[41–43,52,53] Although we are not intend to study the intrinsic transport mechanism of electrolyte-based OFETs, we investigate the active layer thickness-dependent performances to avoid overestimation of the calculated electrical conductivity and to compare the doping thickness of electrolyte-gated OFETs with typical SiO_2. **Figure 7** displays the active film thickness-dependent mobility of PBTTT- and P3HT-based OFET with PMMA/[EMIM][TFSI] dielectric layer. It was observed that the

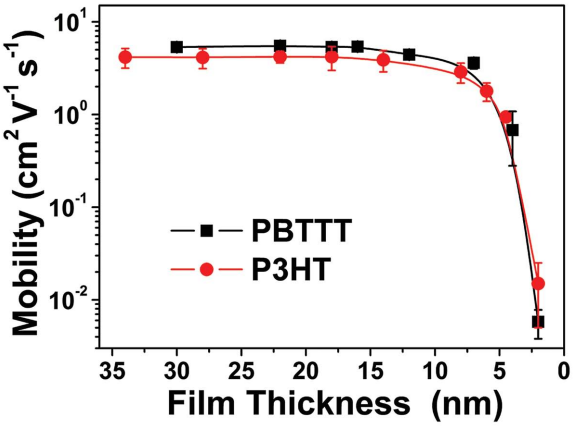

Figure 7. Thickness-dependent mobility of PBTTT and P3HT OFETs with electrolyte dielectric layer. The mobility, extracted from transfer characteristics based on OFETs with PMMA/[EMIM][TFSI] electrolyte dielectric layer, is an average over five different transistors. The operating voltage $V_{DS} = -1$ V.

device performance decreases obviously when the thickness is lower than 16 nm. Therefore, the doping thickness in the electrolyte-gated device is higher than that in typical OFETs with SiO_2 dielectric layer (4–6 nm), but the electrical-field-induced "bulk doping" in electrolyte FETs does not necessarily occur in the entirety of the film. Considering such kind of "bulk doping" using ionic liquid gating, we calculated the conductivity of the electrolyte-based devices with thickness of 16 nm.

Figure 8 summarizes the thermoelectric properties of OFETs with both SiO_2 and PMMA/[EMIM][TFSI] electrolyte dielectric layer. For PBTTT-based device, although OFETs with electrolyte and SiO_2 dielectric layers exhibit different S–σ trade-off relationships, they follow the same S–N_{ind} trend, i.e., the data for the electrolyte- gated devices appear to be an extension of the S–N_{ind} seen for the SiO_2 gate dielectric to higher values of N_{ind} (Figure 8a,b). As a result, the electrical conductivity of PBTTT OFETs based on the electrolyte dielectric layer reached 3.7 S cm^{-1} at a carrier concentration of 2×10^{12} cm^{-2}, whereas the conductivity of OFETs based on the SiO_2 dielectric layer remains 0.1 S cm^{-1} at the same carrier concentration (Figure 8f), which has increased more than 30-fold. Since the conductivity is determined by the carrier concentration and mobility, the increased conductivity of the OFETs based on the electrolyte dielectric layer at a fixed carrier concentration is ascribed to the enhanced carrier mobility (3.3–5.6 cm^2 V^{-1} s^{-1}) over the typical SiO_2 dielectric-based devices (≈0.1 cm^2 V^{-1} s^{-1}) for PBTTT. For P3HT based devices, the electrical conductivity increases from 0.02 to 3.3 S cm^{-1} (Figure 8f), which is consistent with the mobility increase (≈0.02 to 1.6–4.8 cm^2 V^{-1} s^{-1}). The higher mobility leads to the relatively higher conductivity for the same N_{ind} and as a result the power factor for the electrolyte-gated device is significantly higher than that of the SiO_2 devices. This result indicates that both SiO_2 and electrolyte-gated OFETs can be used to probe thermoelectric properties of organic semiconductors in different carrier density regimes. Moreover, the improvement of carrier mobility facilitates the optimization of thermoelectric performances.

Based on a combination of thermoelectric measurement and electrical field modulation, the effective modulation of thermoelectric power factor based on different semiconductors with OFETs geometry can be achieved, which enables the investigation of the thermoelectric properties of organic semiconductors. This methodology should be applicable to various high mobility

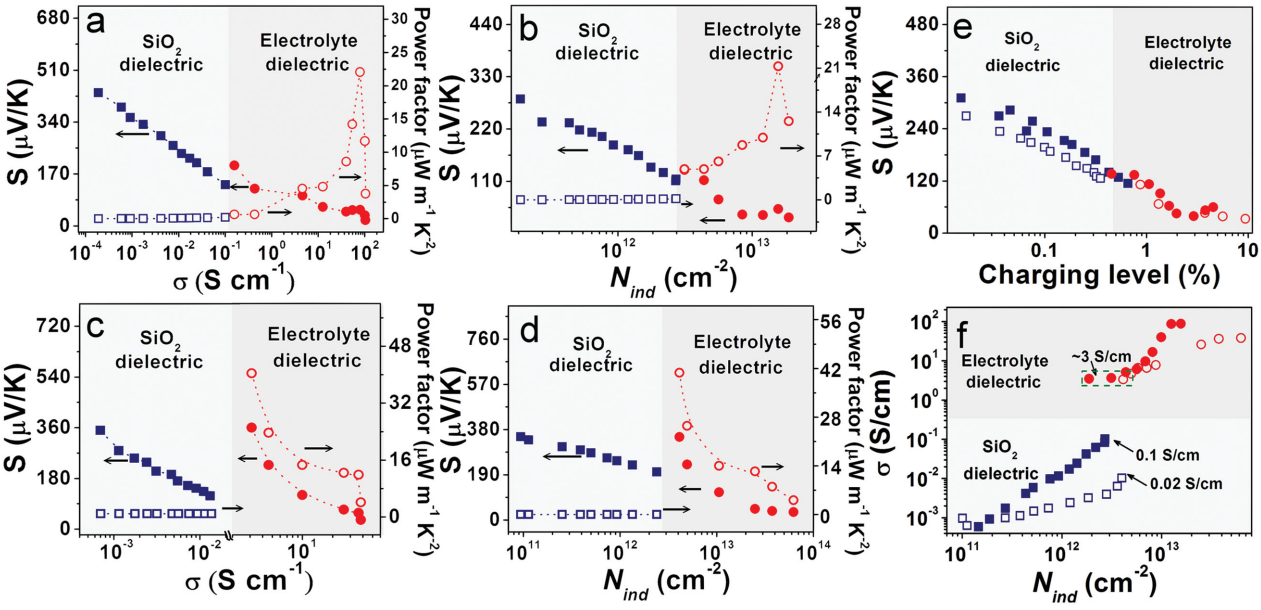

Figure 8. Thermoelectric properties of OFETs with electrolyte dielectric layers. Seebeck coefficient (filled symbols) and thermoelectric power factor (open symbols) as a function of a,c) electrical conductivity and b,d) carrier density for a,b) PBTTT and c,d) P3HT-based OFETs with SiO_2 dielectric (navy square) and PMMA/[EMIM][TFSI] electrolyte dielectric layer (red dot). e) and f) summarized the Seebeck coefficient as a function of charging level for PBTTT (filled symbols) and P3HT- (open symbols) based OFETs with SiO_2 dielectric and PMMA/[EMIM][TFSI] electrolyte dielectric layer, respectively.

organic semiconductors. OFET could therefore provide us a feasible way to screen promising organic thermoelectric materials from hundreds of well-investigated organic semiconductors. Notably, the investigation of the relationship among the electrical conductivity, carrier concentration, charging level, and Seebeck coefficient in the FET geometry can facilitate an optimized chemical doping of organic materials. However, the figure of merit (ZT) is determined by S, σ, and κ while the thermal conductivity is difficult to be obtained with OFETs. As a consequence, electrical-field-induced modulation of thermoelectric properties in OFETs is not mean to replace chemically doping of organic semiconductors for practical applications, but rather provides information for chemical doping towards maximized thermoelectric performances.

3. Conclusions

We have demonstrated a systematic study of utilizing OFET with both SiO_2 and electrolyte dielectric layer to achieve effective modulation of thermoelectric properties based on a series of p- and n-type organic semiconductors. Benefiting from fine-tuning of carrier concentration and charging level over a wide range by varying the applied gate voltage, the extracted thermoelectric performances from OFETs are consisted with the results of chemically doped films. In particular, it allows systematic investigation of trade-off relationship among carrier concentration, charging level, electrical conductivity, and Seebeck coefficient in a FET structure. Our results therefore offer an efficient strategy to accelerate the search for promising thermoelectric materials by scanning through a large variety of organic semiconductors with prominent charge transport properties.

4. Experimental Section

Fabrication of OFET with SiO_2Dielectric Layer: Four semiconductors, including PBTTT (Solarmer, M_w = 3.4 w g mol^{-1}), P3HT (Sigma–Aldrich, M_w = 1.8 w g mol^{-1}), NDI3HU-DTYM2, and NDI(2OD)(4t-BuPh)-DTYM2 (synthesized according to the previous report[54,55]) were used to fabricate OFETs on highly doped silicon substrate with a 300 nm thick thermally SiO_2. The source-drain gold electrodes were sputtered and patterned by a lift off technique. The channel lengths were varied from 200 to 600 μm and the channel width was maintained at 1.2 cm. Before organic semiconductors deposition, the substrates were treated with octadecyltrichlorosilane (OTS) in a vacuum oven. The organic films were deposited by typical spin-coating process and followed by annealing treatment. TEM measurements were performed using JEM-1011.

Fabrication of OFETs with Electrolyte Dielectric Layer: A 150 wt% ion liquid ([EMIM][TFSI]; Sigma–Aldrich) added to PMMA (80 mg mL^{-1}, butyl acetate) was prepared for casting the polymer-electrolyte layer. Corning 7059 glass was applied as the substrate for the electrolyte-based top-gated PBTTT and P3HT OFETs after cleaning in an ultrasonic bath with deionized water, acetone, and isopropanol. 30 nm Au source and drain electrodes were deposited via typical thermal evaporation. Then, the PBTTT and P3HT thin film were deposited spin-coating process at a speed of 4000 rpm.[56] After annealing treatment, PMMA/[EMIM][TFSI] layer were prepared by spin-coating their solution onto the semiconductor films and dried in N_2 glove box, followed by the Al evaporation to serve as the gate electrodes.

Electrical Measurement of OFETs: The FET characteristics were measured at room temperature by a Keithley 4200-SCS semiconductor parameter analyzer. Capacitance-frequency measurements of electrolyte dielectric film were carried out using metal-insulator-metal structure with Keithley 4200-SCS and NF ZM2372 LCR parameter analyzer.

Thermoelectric Property Measurement of OFETs: The Seebeck coefficient is obtained from equation: $S = V_{therm}/\Delta T$, where V_{therm} is the thermoelectric voltage generated when two ends of a sample are maintained at a temperature different (ΔT). The thermoelectric voltage V_{therm} was measured with the Keithley 4200-SCS and the gate voltage was supplied by an Agilent B2901A. The temperature difference was introduced between source and drain electrodes by two Peltier and monitored using an infrared camera FLIR A300.

Chemical Doping of Organic Semiconductors: The PBTTT, P3HT, NDI3HU-DTYM2, and NDI(2OD)(4t-BuPh)-DTYM2 films were doped with $NOPF_6$, graphene oxide, ammonia and hydrazine, respectively. The chemical doping processes of PBTTT and P3HT were performed according to the previous reports.[25,33] For NDI3HU-DTYM2 and NDI(2OD)(4t-BuPh)- DTYM2 film, the chemical doping was carried out by exposing the film to sublimated ammonia and hydrazine vapor.

Supporting Information

Supporting Information is available from the Wiley Online Library or from the author.

Acknowledgements

This research was financially supported by the Major State Basic Research Development Program (2013CB632500), the Strategic Priority Research Program of the Chinese Academy of Sciences (XDB12010000), and the National Natural Science Foundation (21422310, 61171055 and 21333011).

Received: December 12, 2014
Revised: March 6, 2015
Published online: April 7, 2015

[1] D. M. Rowe, *Thermoelectrics Handbook: Macro to Nano*, CRC Press, Boca Raton, FL, USA **2006**.
[2] W. A. Wong, D. J. Anderson, K. L. Tuttle, R. C. Tew, *Status of NASA's Advanced Radioisotope Power Conversion Technology Research and Development*, Albuquerque, New Mexico, USA, **2005**.
[3] H. Nemoto, M. Kishi, T. Hamao, M. Yamamoto, S. Sudou, M. Mandai, S. Yamamoto, presented at XVIII Int. Conf. ThermoelectricsBaltimore, MD, USA **1999**.
[4] G. J. Snyder, E. S. Toberer, *Nat. Mater.* **2008**, *7*, 105.
[5] N. Savage, *Nat. Photonics* **2009**, *3*, 541.
[6] L. E. Bell, *Science* **2008**, *321*, 1457.
[7] J. h. Yang, H.-L. Yip, A. K. Y. Jen, *Adv. Energy Mater.* **2013**, *3*, 549.
[8] Q. Zhang, Y. M. Sun, W. Xu, D. B. Zhu, *Adv. Mater.* **2014**, *26*, 6829.
[9] T. O. Poehler, H. E. Katz, *Energy Environ. Sci.* **2012**, *5*, 8110.
[10] Q. Zhang, Y. M. Sun, W. Xu, D. B. Zhu, *Energy Environ. Sci.* **2012**, *5*, 9639.
[11] O. Bubnova, Z. U. Khan, A. Malti, S. Braun, M. Fahlman, M. Berggren, X. Crispin, *Nat. Mater.* **2011**, *10*, 429.
[12] O. Bubnova, Z. U. Khan, H. Wang, S. Braun, D. R. Evans, M. Fabretto, P. Hojati-Talemi, D. Dagnelund, J.-B. Arlin, Y. H. Geerts, S. Desbief, D. Breiby, J. Andreasen, R. Lazzaroni, W. Chen, I. Zozoulenko, M. Fahlman, P. J. Murphy, M. Berggren, X. Crispin, *Nat. Mater.* **2014**, *13*, 190.
[13] G.-H. Kim, L. Shao, K. Zhang, K. P. Pipe, *Nat. Mater.* **2013**, *12*, 719.

[14] T. Park, C. Park, B. Kim, H. Shin, E. Kim, *Energy Environ. Sci.* **2013**, *6*, 788.
[15] M. He, J. Ge, Z. Lin, X. Feng, X. Wang, H. Lu, Y. Yang, F. Qiu, *Energy Environ. Sci.* **2012**, *5*, 8351.
[16] O. Bubnova, M. Berggren, X. Crispin, *J. Am. Chem. Soc.* **2012**, *134*, 16456.
[17] A. J. Heerger, *Synth. Met.* **2002**, *125*, 23.
[18] C.-K. Mai, R. A. Schlitz, G. M. Su, D. Spitzer, X. Wang, S. L. Fronk, D. G. Cahill, M. L. Chabinyc, G. C. Bazan, *J. Am. Chem. Soc.* **2014**, *136*, 13478.
[19] B. Russ, M. J. Robb, F. G. Brunetti, P. L. Miller, E. E. Perry, S. N. Patel, V. Ho, W. B. Chang, J. J. Urban, M. L. Chabinyc, C. J. Hawker, R. A. Segalman, *Adv. Mater.* **2014**, *26*, 3473.
[20] Y. M. Sun, P. Sheng, C. A. Di, F. Jiao, W. Xu, D. Qiu, D. B. Zhu, *Adv. Mater.* **2012**, *24*, 932.
[21] O. Bubnova, X. Crispin, *Energy Environ. Sci.* **2012**, *5*, 9345.
[22] M. He, F. Qiu, Z. Q. Lin, *Energy Environ. Sci.* **2013**, *6*, 1352.
[23] N. Dubey, M. Leclerc, *J. Poly. Sci., Part B: Polym. Phys.* **2011**, *49*, 467.
[24] R. A. Schlitz, F. G. Brunetti, A. M. Glaudell, P. L. Miller, M. A. Brady, C. J. Takacs, C. J. Hawker, M. L. Chabinyc, *Adv. Mater.* **2014**, *26*, 2825.
[25] Q. Zhang, Y. M. Sun, F. Jiao, J. Zhang, W. Xu, D. B. Zhu, *Synth. Met.* **2012**, *162*, 788.
[26] H. Ohta, Y. Masuoka, R. Asahi, T. Kato, Y. Ikuhara, K. Nomura, H. Hosono, *Appl. Phys. Lett.* **2009**, *95*, 113505.
[27] W. Liang, A. I. Hochbaum, M. Fardy, O. Rabin, M. Zhang, P. Yang, *Nano Lett.* **2009**, *9*, 1689.
[28] K. P. Pernstich, B. Rossner, B. Batlogg, *Nat. Mater.* **2008**, *7*, 321.
[29] H. Ohta, T. Mizuno, S. Zheng, T. Kato, Y. Ikuhara, K. Abe, H. Kumomi, K. Nomura, H. Hosono, *Adv. Mater.* **2012**, *24*, 740.
[30] D. Venkateshvaran, A. J. Kronemeijer, J. Moriarty, D. Emin, H. Sirringhaus, *APL Mater.* **2014**, *2*, 032102.
[31] A. von Mühlenen, N. Errien, M. Schaer, M.-N. Bussac, L. Zuppiroli, *Phys. Rev. B* **2007**, *75*, 115338.
[32] D. Venkateshvaran, M. Nikolka, A. Sadhanala, V. Lemaur, M. Zelazny, M. Kepa, M. Hurhangee, A. J. Kronemeijer, V. Pecunia, I. Nasrallah, I. Romanov, K. Broch, I. McCulloch, D. Emin, Y. Olivier, J. Cornil, D. Beljonne, H. Sirringhaus, *Nature* **2014**, *515*, 384.
[33] Y. Gao, H. L. Yip, K. S. Chen, K. M. O'Malley, O. Acton, Y. Sun, G. Ting, H. Chen, A. K. Jen, *Adv. Mater.* **2011**, *23*, 1903.
[34] Y. Xuan, X. Liu, S. Desbief, P. Leclère, M. Fahlman, R. Lazzaroni, M. Berggren, J. Cornil, D. Emin, X. Crispin, *Phys. Rev. B* **2010**, *82*, 115454.
[35] Q. Zhang, Y. M. Sun, W. Xu, D. B. Zhu, *Macromolecules* **2014**, *47*, 609.
[36] H. Shimotani, G. Diguet, Y. Iwasa, *Appl. Phys. Lett.* **2005**, *86*, 022104.
[37] J. Sun, M. L. Yeh, B. J. Jung, B. Zhang, J. Feser, A. Majumdar, H. E. Katz, *Macromolecules* **2010**, *43*, 2897.
[38] M. J. Panzer, C. D. Frisbie, *Adv. Funct. Mater.* **2006**, *16*, 1051.
[39] J. H. Cho, J. Lee, Y. Xia, B. Kim, Y. He, M. J. Renn, T. P. Lodge, C. Daniel Frisbie, *Nat. Mater.* **2008**, *7*, 900.
[40] J. Lee, L. G. Kaake, J. H. Cho, X.-Y. Zhu, T. P. Lodge, C. D. Frisbie, *J. Phys. Chem. C* **2009**, *113*, 8972.
[41] A. Laiho, L. Herlogsson, R. Forchheimer, X. Crispin, M. Berggren, *Proc. Natl. Acad. Sci.* **2011**, *108*, 15069.
[42] M. J. Panzer, C. D. Frisbie, *J. Am. Chem. Soc.* **2007**, *129*, 6599.
[43] S. H. Kim, K. Hong, W. Xie, K. H. Lee, S. Zhang, T. P. Lodge, C. D. Frisbie, *Adv. Mater.* **2013**, *25*, 1822.
[44] M. Krüger, M. R. Buitelaar, T. Nussbaumer, C. Schönenberger, L. Forró, *Appl. Phys. Lett.* **2001**, *78*, 1291.
[45] Y. Y. Hu, N. Berdunov, C. A. Di, I. Nandhakumar, F. J. Zhang, X. K. Gao, D. B. Zhu, H. Sirringhaus, *ACS Nano* **2014**, *8*, 6778.
[46] G. Kim, K. P. Pipe, *Phys. Rev. B* **2012**, *86*, 085208.
[47] D. Oberhoff, K. P. Pernstich, D. J. Gundlach, B. Batlogg, *IEEE Trans. Electron Devices* **2007**, *54*, 17.
[48] H. Fritzsche, *Solid State Commun.* **1971**, *9*, 1813.
[49] W. C. Germs, K. Guo, R. A. J. Janssen, M. Kemerink, *Phys. Rev. Lett.* **2012**, *109*, 016601.
[50] N. Mateeva, H. Niculescu, J. Schlenoff, L. R. Testardi, *J. Appl. Phys.* **1998**, *83*, 3111.
[51] W. Brutting, C. Adachi, *Physics of Organic Semiconductors*, Wiley-VCH, Germany **2012**.
[52] J. D. Yuen, A. S. Dhoot, E. B. Namdas, N. E. Coates, M. Heeney, I. McCulloch, D. Moses, A. J. Heeger, *J. Am. Chem. Soc.* **2007**, *129*, 14367.
[53] T. G. Bäcklund, H. G. O. Sandberg, R. Österbacka, H. Stubb, *Appl. Phys. Lett.* **2004**, *85*, 3887.
[54] Y. B. Hu, X. K. Gao, C. A. Di, X. D. Yang, F. Zhang, Y. Q. Liu, H. X. Li, D. B. Zhu, *Chem. Mater.* **2011**, *23*, 1204.
[55] Y. B. Hu, Y. K. Qin, X. K. Gao, F. J. Zhang, C. A. Di, Z. Zhao, H. X. Li, D. B. Zhu, *Org. Lett.* **2012**, *14*, 292.
[56] F. J. Zhang, C. A. Di, N. Berdunov, Y. B. Hu, X. K. Gao, Q. Meng, H. Sirringhaus, D. B. Zhu, *Adv. Mater.* **2013**, *25*, 1401.